Further Work on Experimental Plagioclase Equilibria and the Skaergaard Liquidus Temperature

Revision 1

P. Thy,[1] C.E. Lesher,[1] and C. Tegner[2]

[1] Department of Geology
University of California,
One Shields Avenue
Davis, CA 95616, USA

[2] Department of Geoscience
University of Aarhus
DK-8000 Aarhus C
Denmark

Manuscript Revised January 3, 2013

Abstract

Equilibria between plagioclase and ferrobasaltic melt in low-pressure, dry melting experiments can be demonstrated near the liquidus. Further analyses of melting experiments using optimized beam conditions reveals that previous data for understanding the Skaergaard intrusion potentially suffered from the analytical inclusion of non-equilibrated components in the average plagioclase compositions. New reversal experiments demonstrate convergence between plagioclase rim compositions in melting and crystallization products for a ferrobasaltic melt and thus support equilibrium relations. The new dataset provides tighter bounds on experimental plagioclase composition and documents composition-dependent partitioning of Na and Ca between plagioclase and melt. Application of the results to modeling the Skaergaard requires only minor adjustments to the previously proposed liquidus temperatures and liquid line of descent.

Keywords: plagioclase, melting experiments, equilibrium, Skaergaard intrusion, liquidus temperature

Introduction

Plagioclase is ubiquitous in low-pressure melting experiments involving ferrobasalts with Skaergaard affinities (e.g., Biggar, 1974; Hoover, 1989; Juster et al., 1989; Snyder et al., 1993; Toplis and Carroll, 1995). Because of sluggish reaction kinetics and difficulties in attaining and demonstrating equilibria, specifically in dry melting experiments, attention is required when products are evaluated and experimental plagioclase are used in petrogenetic modeling (Johannes, 1978; Johannes and Koepke, 2001; Morse, 2010).

Melting experiments are typically performed on a fine powder of the rock of interest (or its synthetic equivalent) pressed into a pellet and inserted directly into a furnace at the desired final melting temperature. The pellet typically equilibrates toward stable equilibria from its original mineral content and compositions within 12 to 24 hour duration. Although equilibrium can normally be demonstrated for olivine and pyroxenes, it is often difficult to obtain and document stable equilibrium for plagioclase. The reason is that the attainment of stable plagioclase equilibrium typically is restricted to the development of narrow marginal mineral zoning and the preservation of unreacted sodic fragments in cores of plagioclase grains (Johannes and Koepke, 2001). In order to account for this, experimentalists direct the electron beam to the marginal parts of plagioclase grains. Despite such caution, published plagioclase analyses still are often associated with large uncertainties particularly for low temperature melting experiments that may be related to the incorporation of unreacted parts in recorded averages.

Johannes and Koepke (2001), therefore, in a study of plagioclase equilibria in melting experiments have expressed the view that most experimental results are not even close to equilibrium, contrary to the opinion of their authors. Another view has recently been voiced by Morse (2010), suggesting that the existing low-pressure experimental plagioclase-melt database suffer from endemic metastable equilibria and is of little use for evaluating equilibrium conditions.

On this background, we re-evaluate our previous plagioclase-melt data (Thy et al., 2006) using new, optimized, high-resolution, back-scattered electron (BSE) images and narrow electron-beam analyses. We confirm that incomplete reactions can explain the large uncertainty in many existing plagioclase-melt data (Grove et al., 1982; Grove and Bryan, 1983; Beard and Lofgren, 1991; Toplis and Carroll, 1995;

Thy et al., 2006) and outline the simple experimental and analytical techniques required for studying basaltic plagioclase-melt equilibrium relations. We further report the positive result of new convergence experiment demonstrating that plagioclase equilibria can be obtained in melting experiments on ferrobasaltic magmas. The improvements in our plagioclase dataset from 2006 have minimal effects on modeling the liquid line of descent for ferrobasaltic magmas (Thy et al., 2006, Thy et al., 2008; Thy et al., 2009b) and on estimating the liquidus temperatures for the Skaergaard intrusion (Thy et al., 2009a).

Experimental Procedures

The experimental products re-examined in this study were originally described by Thy et al. (2006) in a study of Skaergaard dikes (FG1). All samples are from dike swarms believed to be associated with the Skaergaard intrusion and its liquid line of descent (Nielsen, 1978). The majority of experiments were performed on chilled margin samples without or with only submicroscopic plagioclase (Am, Bm, and Cm; Brooks and Nielsen, 1990). The remaining sample (Dc) was from the center of a dike that contains fresh groundmass plagioclase (Brooks and Nielsen, 1978). All samples were finely powdered to an estimated maximum grain size of 10 μm and were not dried above ambient temperature.

The new data reported here are for a subset of the original one-atmosphere experiments all of which represent near liquidus conditions. These run products contain between 94 and 80 % melt, 5 to 12 % plagioclase, and small amounts of olivine (all by weight). In addition, we present in Table 1 results of one-GPa melting experiments performed in a standard ½" piston-in-cylinder press with powders of Am and Cm contained in graphite capsules. The high-pressure experimental products contain 60 to 70 % melt, 24 to 30 % high-Ca pyroxene, and 6 to 11 % plagioclase. Details of the experimental conditions for the new and previous analytical results are summarized in Table 1.

All experiments, except one (FG1Cm-19), were melting experiments, meaning that the powders were directly brought from room temperature to the desired experimental temperature and held there until quenched in air. The experimental durations varied between 22 and 94 hours. The one–atmosphere experiments used the standard wire-loop techniques in a vertical quench furnace with gas-mixing

control at the fayalite-magnetite-quartz oxygen buffer. For the high-pressure experiments the assembly consisted of a CaF_2 pressure medium surrounding a graphite resistance heater, capsule and internal spacers of MgO. Temperature was controlled within ±5º C using a D-type thermocouple (without corrections for the pressure effect on emf readings), and thermal quenching was achieved by cutting power to the heater.

The results of a convergence experiment are summarized in Table 2 using a titanium-rich ferrobasalt from the East Greenland plateau lavas. The first experiment was a melting experiment ramped at >300 ^{o}C/min to the dwell temperature of 1132^{o}C, below the liquidus temperature and kept there for 24 hours after which the product was quenched in water. The second experiment was a dynamic crystallization experiment made by letting the temperature oscillate around the expected liquidus decreasing the cooling rates with each cycle (5 ^{o}C/min and 1 ^{o}C/min). The final dwell temperature was at 1145 ^{o}C for duration of 76 hours (see Table 2 for details).

Analytical Procedures

The selected experimental products were previously analyzed in the early 1990's using a CAMECA SX-50 electron microprobe. At that time the mineral phases were analyzed using a narrow beam (1-2 μm) and glasses were analyzed using a broad beam of 10-μm diameter to avoid sodium loss. The analytical procedures used by Thy et al. (2006) were representative of common strategies used for analyzing products of melting experiments involving plagioclase (e.g., Drake, 1976; Kinzler and Grove, 1992). It is, however, important to note that the BSE image technique used by Thy et al. (2006) was optimized to distinguish among all silicate phases, including the pyroxenes, and by so doing was unable clearly to detect small differences in plagioclase compositions. Consequently, we found and noted large variations in anorthite-content with standard deviations often reaching 4-6 % An (1σ). Such large standard deviations were attributed to incorporation of unreacted cores in the average value in marked contrast to coexisting olivine with standard deviations normally well below 0.5 % Fo (1σ) (Thy et al., 2006).

The experimental near-liquidus products of Thy et al. (2006) selected for this study contain plagioclase contents sufficiently high to allow multiple analyses of

grain rims. The new analyses were performed using a CAMECA SX-100 electron microprobe, employing the same mineral standards and beam conditions as for the 2006 study. However, this time the back-scattered electron (BSE) imaging resolution and contrast were optimized to allow us to distinguish plagioclase compositions with an absolute variation of 1-2 wt. % Na_2O, or about 10 % An-content (Table 1). Table 3 summarizes the new analytical results, while the previous dataset can be found in Thy et al. (2006). The products of the convergence experiment were analyzed using the same method as used for reanalyzing the older experimental products with the results summarized in Table 2.

Results and Discussion

The BSE images summarized in Figure 1 illustrate that it is possible to distinguish between plagioclase rims and cores based on mean-atomic-density variation. The cores appear as irregular dark regions with low mean-atomic density (high sodium). The overall shape varies from large (~50 to 100 μm), highly irregular, sieve-textured grains (FG1Am and FG1Cm; Figure 1) to smaller (10-50 μm) grains with irregular and embayed margins (FG1Bm and FG1Dc; Figure 1) to partially faceted growth surfaces (e.g., FG1Dc; Figure 1). The cores often contain minute grains of oxides. Sieve-textured grains sometime outline an overall rectangular fabric reaching about 100 μm in their longest dimension. The presence of compositionally identical rims through sieve-textured grains suggests connectivity allowing reaction and precipitation of compositionally similar plagioclase.

The contacts between rims and cores are in all cases highly irregular, suggesting partial resorption followed by precipitation of new plagioclase during heating as proposed by Johannes and Koepke (2001). There is no evidence of exchange between plagioclase cores and rims on the time scale of the experiments, consistent with the low interdiffusivities for plagioclase components (Grove et al., 1984).

There are a couple of experimental constraints and observations that have important bearing on the origin of the plagioclase textures. The original starting materials are powders containing very fine (<10 μm diameter) fragments much smaller than many of the sieve plagioclase grains. Moreover, in thin section these sieve plagioclases are optically continuous and occasionally include euhedral olivine (FG1Am-9; Figure 1) or vice versa (FG1Am and FG1Bm; Figure 1). These

observations suggest that sieve-textured plagioclase nucleated and grew rapidly under supercooled conditions during heating. On approaching the final dwell temperature the grains were partially resorbed and/or overgrown by more An-rich, near-liquidus plagioclase. This interpretation also applies to sieve textured plagioclases observed in natural basalts attributed to constitutional supercooling during magma mixing or rapid ascent (Dungan and Rhodes, 1978; Tsuchiyama and Takahashi, 1983; Tsuchiyama, 1985; Nelson and Montana, 1992). It is noteworthy that sieve plagioclase are scarce in experiments using starting material from dike centers, i.e. FG1Dc, presumably because the presence of plagioclase crystal fragments ("seeds") did not present a barrier to crystal nucleation.

In contrast to our one-atmosphere experiments, plagioclase in the one-GPa products show ubiquitous faceted rim growth sometimes as overgrowths on sieve-textured plagioclase (FG1Am-1-8; Figure 1). Overall these high-pressure products display greater textural equilibration consistent with enhanced kinetics of reaction and diffusion at elevated pressure and perhaps the presence of small amounts of water remaining in the original starting material (e.g. Johannes, 1978; Johannes and Koepke, 2001).

Assessment of plagioclase-melt equilibrium

Our refined operating conditions for BSE imaging of experimental products clearly distinguishes plagioclase rims with higher mean-atomic density (higher calcium-content) from cores with lower mean-atomic density (higher sodium-contents) (Figure 1). The width of rims varies from a few microns to 20 μm (Figure 1) and thus enables representative analyses to be obtained using an optimally sized electron beam without interferences from melt and plagioclase core material. Table 3 summarizes the new core and rim analyses of plagioclase. The new rim compositions are systematically more calcic (An_{64-80}) than the cores (An_{53-70}), and, likewise, often more calcic than the average compositions reported by Thy et al. (2006) (An_{58-73}). The latter averages consistently lie between the new core and rim compositions, although for starting materials FG1Bm and FG1Dc the old averages are indistinguishable from the new rim compositions within uncertainties. We can now show that some of our previous plagioclase data represented to varying extents analytical mixtures of core and rim that skewed the average An-contents to lower

values. This problem was more severe in experimental products in which there were only very thin rims of new growth on relict plagioclase. Figure 2 compares the new and old data as a function of final dwell temperature. The new data for rims approach the empirical fit of Thy et al. (2009a) based on experimental liquidus plagioclase from 450 experiments on North Atlantic ferrobasalts.

The plagioclase grains in the melting product of the convergence experiment showed the same distribution between sodic cores of $An_{61.4}$ and calcic rims of $An_{67.6}$ found for the Skaergaard dikes (Table 2). The product of the dynamic crystallization experiments contained unzoned plagioclase of $An_{68.9}$ and thus converged within the analytical uncertainty to the results of the melting experiment, clearly supporting the attainment of equilibria in the melting experiments. The distribution coefficient for sodium and calcium between plagioclase and liquid was likewise well reversed by the convergence experiment (Table 2).

Reversal of the plagioclase liquidus was also demonstrated by Thy et al. (2006) for dike composition FG1Cm (their table 1, experiments 13 and 19) to within ±2-3 ^{o}C. Experiment 13 was a melting experiment brought up from ambient to above the liquidus, while 19 was a crystallization experiment that was kept above the liquidus for 30 minutes before being lowered to below plagioclase saturation. The composition of plagioclase rims in this crystallization experiment ($An_{70.9}$; FG1Cm-19, Table 1) is identical within uncertainty to near-liquidus rim compositions in our melting experiments ($An_{69.3\text{-}70.6}$; FG1Cm-10 and FG1Cm-8, Table 1).

An additional test of reversibility is possible by comparing the crystallization experiments of Toplis and Carroll (1995) to the melting experiments of Thy et al. (2006) for the same starting composition (FG1C). The natural dike sample used by Thy et al. (2006) was from the chilled margin (Brooks and Nielsen, 1990) of the same dike for which a central composition was synthesized by Toplis and Carroll (1995) from reagent-grade oxides and carbonates, only excluding MnO and P_2O_5. In table 1 of Thy et al. (2006) the compositions of the two samples are given as FG1Cm and FG1Cc, respectively. The plagioclase composition was $An_{70.9}$ at a liquidus temperature of 1164±4 ^{o}C in the crystallization experiments of Toplis and Carroll (1995), which is similar to the liquidus plagioclase ($An_{71.4}$; 1168±3 ^{o}C) in our melting experiment (Table 1). This demonstrates excellent interlaboratory agreement

and provides further evidence that near liquidus equilibrium was attained in both these melting and crystallization experiments.

Distribution Coefficients

The compound distribution coefficient $K_{D,std}$ for the new plagioclase rim analyses and the melt (glass) analyses of Thy et al. (2006) vary from 0.80 to 1.09, where $K_{D,std}$ is defined conventionally on an atomic basis as $(Na/Ca)^{pl}/(Na/Ca)^{liq}$. A similar coefficient ($K_{D,Morse}$) based on the distribution of anorthite (An) and albite (Ab) components between melt and plagioclase varies from 0.38 to 0.53, where the An and Ab contents for the melt come from the normative plagioclase composition of a standard CIPW norm calculation (Morse, 2010). For both definitions, there is a systematic increase in K_D that generally correlates positively with iron and titanium contents of the melts as well as negatively with melting temperature (Thy et al., 2006; Table 1). The similarly defined K_D's for the reversal experiment (Table 2) are 1.06-0.95 ($K_{D,std}$) and 0.46-0.43 ($K_{D,Morse}$). The results are shown in Figure 3, using the binary linear partition diagram approach advocated by Morse (2000, 2010). Morse argues that true equilibrium for all low-pressure plagioclase-melt pairs requires a $K_{D,Morse}$ of ~0.26 as shown for the simple albite-anorthite and albite-anorthite-diopside systems (e.g., Bowen, 1913, 1915). In contrast, the present results suggest a strong compositional control on $K_{D,Morse}$ for evolved basalt compositions (as is the case for $K_{D,std}$). This is also predicted by the MELTS algorithm (Figure 3) and was observed by Toplis and Carroll (1995) in their experimental study of a Skaergaard dike.

Pressure Effects

Morse (2010) showed that plagioclase $K_{D,Morse}$ for high-alumina basaltic magmas depends on pressure and found that extrapolation of data from 0.5 to 1 GPa (Fram and Longhi, 1992; Morse et al., 2004) to one atmosphere agreed well with the K_D for the albite-anorthite-diopside system. A similar evaluation of our experimental data on the FG1 dikes (Table 1) shows that $K_{D,Morse}$ (and $K_{D,std}$) is weakly dependent on pressure between one-atmosphere and one-GPa. Moreover, for such ferrobasaltic magmas the liquidus temperature of augite increases markedly with pressure at the expense of plagioclase until the latter ceases to crystallize at intermediate pressures

(0.8-1 GPa) (Green and Ringwood, 1967; Bender et al., 1978; Thy, 1991). In contrast, high-aluminous basaltic and jotunitic magmas retain plagioclase on or near the liquidus to high crustal pressures (Emslie and Lindsley, 1968; Fram and Longhi, 1992; Morse, 2010). This is another timely reminder that the phase relations for ferrobasaltic magmas relevant to discussions of the Skaergaard intrusion are fundamentally different from the high-alumina magmas of the Kiglapait intrusion (Morse et al., 2004; Morse, 2010).

Liquidus temperature of the Skaergaard Intrusion

The principal motivation for the empirical plagioclase thermometer of Thy et al. (2009a) was to constrain the thermal history of the Skaergaard intrusion from cumulus plagioclase composition. The experimental database of plagioclase-melt pairs used for the model included about 450 one-atmosphere melting experiments performed on 50 different North Atlantic basaltic rocks; only 9 of the starting materials were Skaergaard-related dikes. The An-contents for plagioclase ranged from a high of 88 to a low of 40, covering most of the compositional range of plagioclase in gabbroic rocks of the Skaergaard intrusion. Regressing the entire dataset for plagioclase An-content (in mole %) versus temperature originally yielded the relation: T (^{o}C) = 899 + 3.6 $*$ An ($\pm$ 20 ^{o}C 1σ). We attributed this large uncertainty to the diversity of basaltic rocks used in the experimental studies and the likely inclusion of some non-equilibrium plagioclase grains in this large dataset. Had we restricted consideration to the subset of near-liquidus experiments with $\geq$ 70 % melt and excluding all our experiments on the Skaergaard-related dikes, the regression would be T (^{o}C) = 933+ 3.2 $*$ An ($\pm$ 18 ^{o}C 1σ). If the regression is forced through the same intersection as in the original regression (An_{30} at 1007 ^{o}C), the fit gives T (^{o}C) = 895 + 3.8 $*$ An ($\pm$ 19 ^{o}C 1σ). Both of these regressions are indistinguishable within error to our original fit to the entire North Atlantic experimental dataset (see Figure 2 for comparison). The rationale for the above forced regression is that the low temperature point is reasonable well constrained by direct melting experiments on final differentiation products of the Skaergaard intrusion (Tilley et al., 1963; Lindsley et al., 1969).

Regardless of which fit is preferred, Figure 2 shows the very close agreement between our new plagioclase rim compositions for the Skaergaard-related dikes and

model compositions. This is reassuring considering that the equation of Thy et al. (2009a) also agreed closely with independent liquidus determinations for other Skaergaard rocks (Hoover, 1989; McBirney and Naslund, 1990) and predictions of forward modeling by Ariskin (2003). These considerations do not resolve the discrepancies between the Thy et al. (2009a) and Morse (2008) plagioclase geothermometers; the latter predicting markedly higher liquidus temperatures during the early stages of Skaergaard evolution, although both models converge to similar temperatures at the Sandwich Horizon end-stage. The estimated high temperature differences between the two thermometers amounts to 58 ^{o}C (equivalent to crystallization of LZa and LZb combined). The uncertainty of the thermometer of Thy et al. (2009a) is ±20 ^{o}C at the 1σ level. The uncertainty in the temperature estimates of Morse (2008) is not available. However since both thermometers are based on the same type of data, it may be reasonable to assume that the uncertainties also are largely similar. Thus, at the 1σ confidence interval, the results are systematically different at the temperatures of the LZ, but converge for the low temperature crystallization interval of the UZ. We hypothesize that the differences in the two thermometers largely arises from the attempt to extrapolate the plagioclase liquidus relations for model Kiglapait magmas (high-alumina basalt) at 0.5 GPa (Morse, 2004) to the low-pressure conditions applicable to Skaergaard (Morse, 2008).

Forward modeling of the liquid line of descent for the Skaergaard intrusion

Given the improved dataset, it is worthwhile to consider the implications for forward modeling of the Skaergaard liquid line of descent. The model presented by Thy et al. (2006, 2009b) was based on our experiments on the Skaergaard-related dikes. Since we have demonstrated that some non-equilibrium plagioclase compositions were present in this dataset, it is prudent to assess their impact on the predicted liquid line of descent. The original calculated modes for the eight near-liquidus, low-pressure melting experiments are given in Table 1. Our revised experimental modes based on the new plagioclase analyses are in close agreement with those of Thy et al. (2006).

The $K_{D,std}$ values used by Thy et al. (2006) in their forward modeling are as expected from Figure 2 slightly higher than the values based on the reanalysis of the

near-liquidus run products. Thy et al. (2006) showed that $K_{D,std}$ depends weakly on temperature ($K_{D,std}$ = 7.61 - 0.0057 * T ^{o}C). The new plagioclase rim analyses give a revised relation ($K_{D,std}$ = 5.35 - 0.0038 * T ^{o}C) predicting systematically lower K_D's although the temperature dependence is similarly weak. For example, the $K_{D,std}$ calculated by Thy et al. (2009b) for preferred model 'A' at 1162 ^{o}C (based on lower zone a) is 1.02 and at 1000 ^{o}C (equivalent with the Sandwich Horizon) is 1.92. Similarly, the $K_{D,std}$ based on the revised regression for Skaergaard like dikes only (Table 1) yields 0.93 and 1.55, respectively. Figure 4 compares model liquid lines of descent for Skaergaard using the new and original (Thy et al., 2009b) parameterization of $K_{D,std}$, respectively. As expected, there is a small shift in plagioclase composition (from An_{70} to An_{72}), but the differences diminish with differentiation. Likewise, the Na_2O content of the Skaergaard magma after ~50% fractional crystallization (~1085 ^{o}C) predicted by the original model is 2.76 wt. % and 2.89 wt. % using the revised calibration, while after 75 % fractional crystallization (~1016 ^{o}C) Na_2O is 3.11 and 3.46 % wt., respectively. It is possible that the effect of these changes in melt composition may slightly affect the liquidus temperature and also the modal proportions; however, the overall effects on the liquid line of descent for the Skaergaard intrusion are inconsequential. These adjustments to the plagioclase compositions bring our revised model into even closer agreement with those of Toplis and Carroll (1996) and Ariskin (2003).

Acknowledgements

PT and CEL are grateful to the Department of Geoscience at the University of Aarhus for hospitality and shelter during writing of this short note. The reanalysis of the Skaergaard melting experiments was expertly performed by Brian Joy (Department of Geology, UC Davis). Critical comments from Don Baker and the official journal reviewers helped us to improve the manuscript. The study was supported in part by the US National Science Foundation under Grant Number NSF-EAR-0208075 (CEL). Any opinions, findings, and conclusions or recommendations expressed in this material are those of the authors and do not necessarily reflect the views of the National Science Foundation. The Willum and Carlsberg Foundations, and the Danish Council for Independent Research, Natural Sciences provided support to CT.

References

Ariskin, A.A. (2003) The compositional evolution of differentiated liquids from the Skaergaard layered series as determined by geochemical thermometry. Russian Journal of Earth Sciences, 5, 1-29.

Beard, J.S. and Lofgren, G.E. (1991) Dehydration melting and water-saturated melting of basaltic and andesitic greenstones and amphibolites at 1, 3, and 6-9 kb. Journal of Petrology, 32, 365-401.

Bender, J. F., Hodges, F. N., and Bence, A. E. (1978) Petrogenesis of basalts from the project FAMOUS area: experimental study from 0 to 15 kilobars. Earth Planetary Science Letters, 41, 277-302.

Biggar, G.M. (1974) Phase equilibrium studies of chilled margins of some layered intrusions. Contributions to Mineralogy and Petrology, 46, 159-167.

Bowen, N.L. (1913) The melting phenomena of the plagioclase feldspars. American Journal of Science, 35 (4^{th} Series), 577-599.

Bowen, N.L. (1915) The crystallization of haplobasaltic, haplodioritic and related magmas. American Journal of Science, 40 (4^{th} Series), 161-185.

Brooks, C.K. and Nielsen, T.F.D. (1978) Early stages in the differentiation of the Skaergaard magma as revealed by closely related suite of dike rocks. Lithos, 11, 1-14.

Brooks, C.K. and Nielsen, T.F.D. (1990) The differentiation of the Skaergaard intrusion. Discussion. Contributions to Mineralogy and Petrology, 104, 244-247.

Drake, M.J. (1976) Plagioclase-melt equilibria. Geochimica et Cosmochimica Acta, 40, 457-465.

Dungan, M.A. and Rhodes, M.J. (1978) Residual glasses and melt inclusions in basalts from DSDP legs 45 and 46: evidence for magma mixing. Contributions to Mineralogy and Petrology, 67, 417-431.

Emslie, R.F. and Lindsley, D.H. (1968) Experimental bearing on the origin of anorthositic intrusions. Carnegie Institution of Washington, Year Book, 67, 108-112.

Fram, M.S. and Longhi, J. (1992) Phase equilibria of dikes associated with Proterozoic anorthosite complexes. American Mineralogist, 77, 605-616.

Ghiorso, M. S. and Sack, R. O. (1995) Chemical mass transfer in magmatic processes. IV. A revised and internally consistent thermodynamic model for the interpolation and extrapolation of liquid-solid equilibria in magmatic systems at elevated temperatures and pressures. Contributions to Mineralogy and Petrology, 119, 197-212.

Green, D.H. and Ringwood, A.E. (1967) The genesis of basaltic magmas. Contributions to Mineralogy and Petrology, 15, 103-190.

Grove, T.L. and Bryan, W.B. (1983) Fractionation of pyroxene-phyric MORB at low pressure: an experimental study. Contributions to Mineralogy and Petrology, 84, 293-309.

Grove, T.L., Baker, M.B., and Kinzler, R.J. (1984) Coupled CaAl-NaSi diffusion in plagioclase feldspar: experiments and applications to cooling rate speedometry. Geochimica et Cosmochimica Acta, 48, 2113-2121.

Grove, T.L., Gerlach, D.C., and Sando, T.W. (1982) Origin of calc-alkaline series lavas at Medicine Lake volcano by fractionation, assimilation and mixing. Contributions to Mineralogy and Petrology, 80, 160-182.

Hoover, J.D. (1989) The chilled marginal gabbro and other contact rocks of the Skaergaard intrusion. Journal of Petrology, 30, 441–476.

Johannes, W. (1978) Melting of plagioclase in the system Ab-An-H_2O and Qz-Ab-An-H_2O at P_{H2O}=5 kbars, and equilibrium problem. Contributions to Mineralogy and Petrology, 66, 295-303.

Johannes, W. and Koepke, J. (2001) Incomplete reaction of plagioclase in experimental dehydration melting of amphibolite. Australian Journal of Earth Sciences, 48, 581-590.

Juster, T.C., Grove, T.L., and Perfit, M.R. (1989) Experimental constraints on the generation of FeTi basalts, andesites, and rhyodacites at the Galapagos spreading center, 85°W and 95°W. Journal of Geophysical Research, 94, 9251-9274.

Kinzler, R.J., Grove, T.L. (1992) Primary magmas of Mid-Ocean Ridge Basalts. 1. Experiments and Methods. Journal of Geophysical Research, 97, 6885-6906.

Lindsley, D.H., Brown. G.M., and Muir, I.D. (1969) Conditions of the ferrowollastonite-ferrohedenbergite inversion in the Skaergaard intrusion, East Greenland. Mineralogical Society of America, Special Paper 2, 193-201.

McBirney, A.R. and Naslund, H.R. (1990) The differentiation of the Skaergaard intrusion. Discussion. Contributions to Mineralogy and Petrology, 104, 235-240.

Morse, S.A. (2000) Linear partitioning in binary solutions. Geochimica et Cosmochimica Acta, 64, 2309-2319.

Morse, S.A. (2008) Toward a thermal model for the Skaergaard liquids. American Mineralogist, 93, 248-251.

Morse, S.A. (2010) A critical comment on Thy et al. (2009b): Liquidus temperatures of the Skaergaard magma. American Mineralogist, 95, 1817-1827.

Morse, S.A., Brady, J.B., and Sporleder, B.A. (2004) Experimental petrology of the Kiglapait intrusion: cotectic trace for the lower zone at 5kb in graphite. Journal of Petrology, 45, 2225-2259.

Nelson, S.T. and Montana, A. (1992) Sieve-textured plagioclase in volcanic rocks produced by rapid decompression. American Mineralogist, 77, 1242-1249.

Nielsen, T.F.D. (1978) The Tertiary dike swarms of the Kangerdlugssuaq area, East Greenland. An example of magmatic development during continental break-up. Contributions to Mineralogy and Petrology, 67, 63-78.

Snyder, D., Carmichael, I.S.E., and Wiebe, R.A. (1993) Experimental study of liquid evolution in a Fe-rich, layered mafic intrusion: constraints of Fe-Ti oxide precipitation on the T-f_{O2} and T-ρ paths of tholeiitic magmas. Contributions to Mineralogy and Petrology, 113, 73-86.

Thy, P. (1991) High and low pressure phase equilibria of a mildly alkalic lava from the 1965 Surtsey eruption: experimental results. Lithos, 26, 223-243.

Thy, P., Tegner, C., and Lesher, C.E. (2009a) Liquidus temperature of the Skaergaard magma. American Mineralogist, 94, 1371-1376.

Thy, P., Lesher, C.E., and Tegner, C. (2009b) The Skaergaard liquid line of descent revisited. Contributions to Mineralogy and Petrology, 157, 735-747.

Thy, P., Lesher, C.E., Nielsen, T.F.D., and Brooks, C.K. (2006) Experimental constraints on the Skaergaard liquid line of descent. Lithos, 92, 154-180.

Thy, P., Lesher, C.E., Nielsen, T.F.D., and Brooks, C.K. (2008) On the Skaergaard intrusion and forward modeling of its liquid line of descent: a reply to "Principles of applied experimental igneous petrology" by Morse, 2008, Lithos 105: 395-399. Lithos, 105, 401-411.

478 Tilley, C.E., Yoder, H.S., and Schairer, J.F. (1963) Melting relations of basalts.
479 Carnegie Institution of Washington Year Book, 62, 77-84.
480 Toplis, M.J. and Carroll, M.R. (1995) An experimental study of the influence of
481 oxygen fugacity on Fe-Ti oxide stability, phase relations, and mineral-melt
482 equilibria in ferro-basaltic systems. Journal of Petrology, 36, 1137-1170.
483 Toplis, M.J. and Carroll, M.R. (1996) Differentiation of Ferro-basaltic magmas
484 under conditions open and closed to oxygen: implications for the Skaergaard
485 intrusion and other natural systems. Journal of Petrology, 37, 837-858.
486 Tsuchiyama, A. (1985) Dissolution kinetics of plagioclase in the melt system
487 diopside-albite-anorthite, and origin of dusty plagioclase in andesites.
488 Contributions to Mineralogy and Petrology, 89, 1-16.
489 Tsuchiyama, A. and Takahashi, E. (1983) Melting kinetics of a plagioclase feldspar.
490 Contributions to Mineralogy and Petrology, 84, 345-354.

Figure and Table Captions

Figure 1. Back-scattered electron images showing plagioclase-melt relations for representative experiments from Table 1. The images are mean-atomic density maps where light plagioclase (usually as rims) is anorthitic and darker plagioclase (usually forming the cores) is more abitic. Ol - olivine.

Figure 2. Plagioclase composition (An mole %) as a function of melting temperature (T ^{o}C). Shown are averages and standard deviations at the 1σ level. Included are the new plagioclase rim compositions from Table 1 compared to plagioclase "averages" reported by Thy et al. (2006). The letters 'A' to 'D' refer to the series of experiments on the FG1 dikes reported in Table 1 and Thy et al. (2006). The dashed black line is the empirical plagioclase thermometer of Thy et al. (2009a) based on 450 one-atmosphere melting experiments on North Atlantic basalts. The solid grey line is a similar regression, but using only those experiments with > 70 % melt and excluding all experiments on the FG1 dikes. The dashed grey line is the regression of this same subset of data, but forced through 1007 ^{o}C and An_{30} as obtained on the original regression.

Figure 3. Binary linear partitioning diagram of Morse (2000) where the mole fraction of anorthite in plagioclase (X^{pl}_{An}) is plotted against the ratio of the mole fraction of albite in plagioclase and liquid, respectively (i.e., $D = X^{pl}_{Ab} / X^{liq}_{Ab}$). X^{liq}_{Ab} is derived from CIPW normative plagioclase composition for the liquid. The slope of D versus X^{pl}_{An} is $-K_{D,Morse}$. Curves for $K_{D,Morse}$ = 0.26 - 0.70 are plotted with 0.26 being the value proposed by Morse (2000, 2010) for plagioclase-melt equilibrium in simple binary (Ab-An), ternary (Ab-An-Di) and natural basaltic systems at low pressure. Deviations from this value are considered due to plagioclase disequilibrium by Morse (2010) and purported to be ubiquitous in one-atmosphere experiments on basaltic systems. Also plotted are our equilibrium one-atmosphere results for FG1 compositions A, B, C and D defining a sloping array that cuts across $K_{D,Morse}$ contours from 0.26 to 0.46, along with data for 1 GPa falling on the 0.60 $K_{D,Morse}$ line. The increase in $K_{D,Morse}$ along the 1-atm array correlates with enrichment in FeO and TiO_2. The grey dashed line is the trend for one-atmosphere

fractional crystallization buffered at FMQ predicted by MELTS (Ghiorso and Sack, 1995) for the initial composition FG1-Cm. The MELTS results extends the trend to even higher $K_{D,Morse}$ shown by the one-atmosphere experiments, consistent with our conjecture that $K_{D,Morse}$ is compositionally dependent in naturally occurring basaltic magmas.

Figure 4. An-content of plagioclase (mole %) versus temperature showing the results of forward modeling the Skaergaard liquid line of descent based on the original parameterization of Thy et al. (2009b) and the new parameterization for $K_{D,std}$ (this study).

Table 1. Run conditions for near-liquidus melting experiments on FG1 dikes starting materials (see Thy et al. 2006), and "new" and "old" (Thy et al., 2006) plagioclase analyses for these run products. All experiments are of the "melting" type, where temperature is ramped to T_{dwell} and quenched after t_{dwell}, except FG1Cm-19 that was held at 1177 ºC (~10 º above the liquidus) for 30 minutes and lowered at 500 ºC/hour to a T_{dwell} of 1168 ºC. The one GPa experiments are new; all 1-atm experiments from Thy et al. (2006).

Table 2. Reversal/convergence experiment for ferrobasaltic magma (East Greenland basalt, GEUS 435068). Melting (JAS-78PT) and dynamic crystallization experiments (JAS-29PTB). All experiments at a f_{O2} of $10^{-9.3}$.

Table 3. Summary of plagioclase analyses for near-liquidus melting experiments on FG1 dikes. See Table 1 for experimental conditions and Thy et al. (2006) for details and the compositions of the coexisting phases.

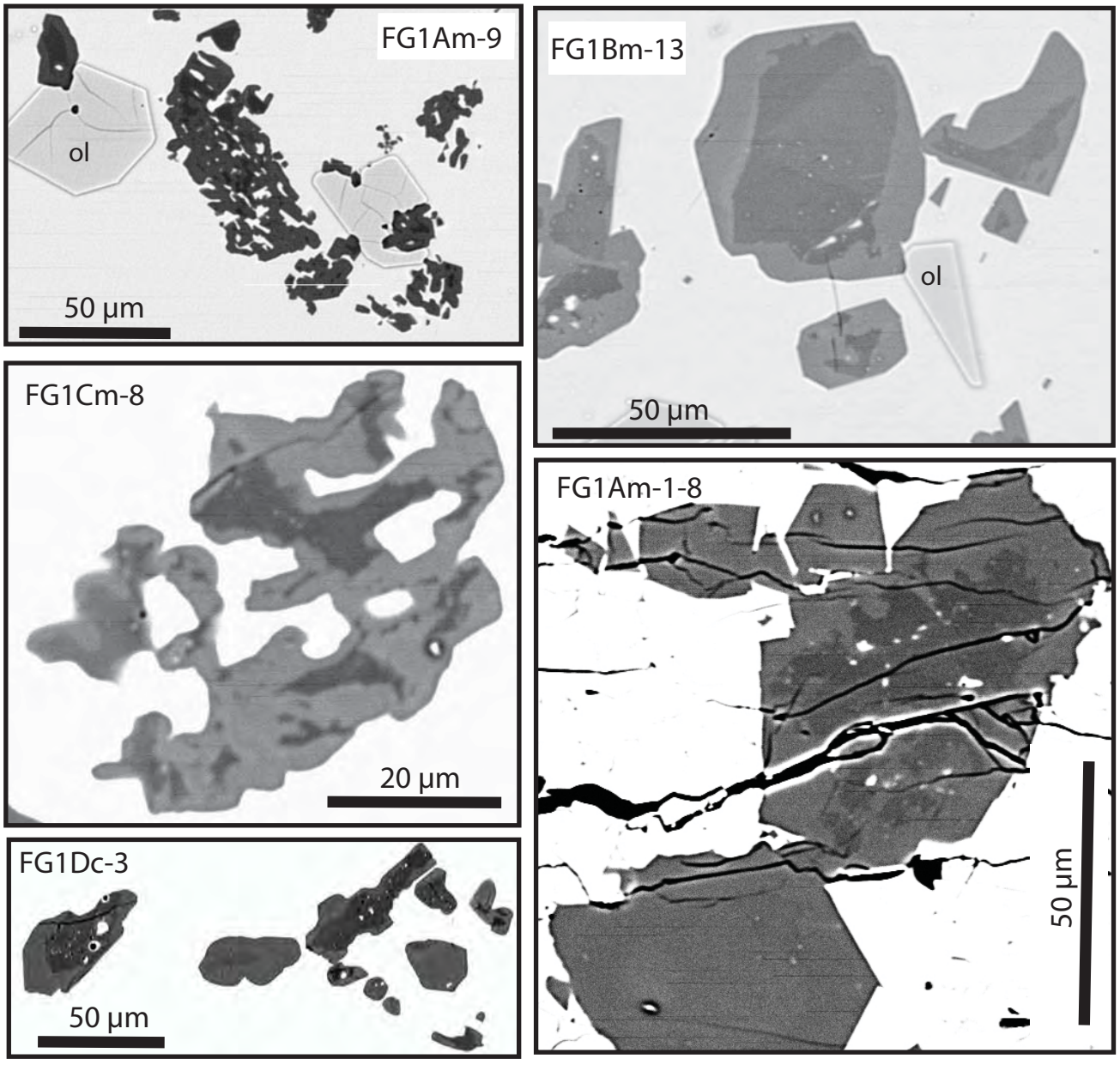
FG1Am-9
ol
50 µm
FG1Bm-13
ol
50 µm
FG1Cm-8
20 µm
FG1Am-1-8
50 µm
FG1Dc-3
50 µm

Figure 1

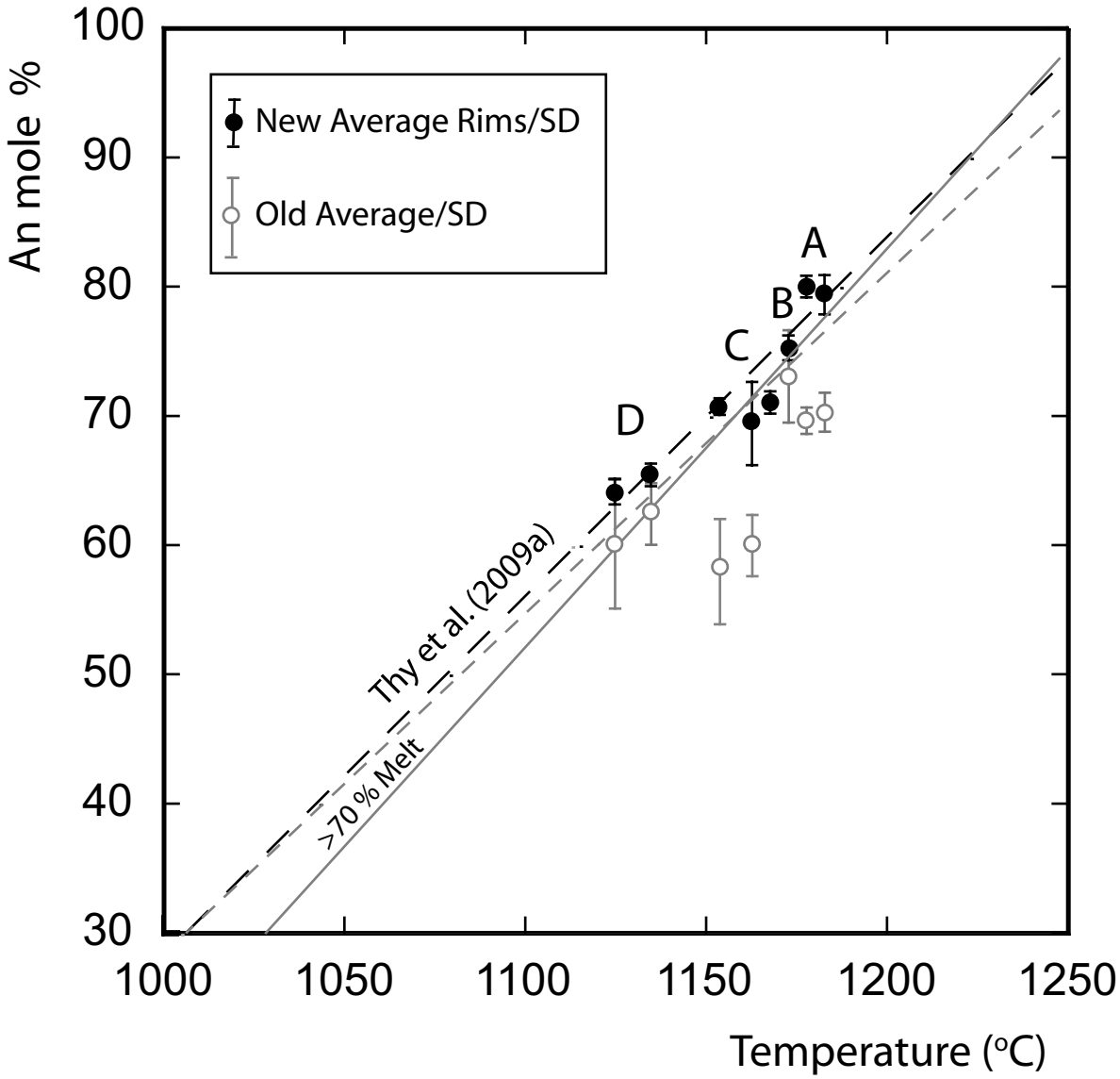
An mole %
100
90
80
70
60
50
40
30
1000
1050
1100
1150
1200
1250
Temperature (°C)
New Average Rims/SD
Old Average/SD
A
B
C
D
Thy et al. (2009a)
>70 % Melt

Figure 2

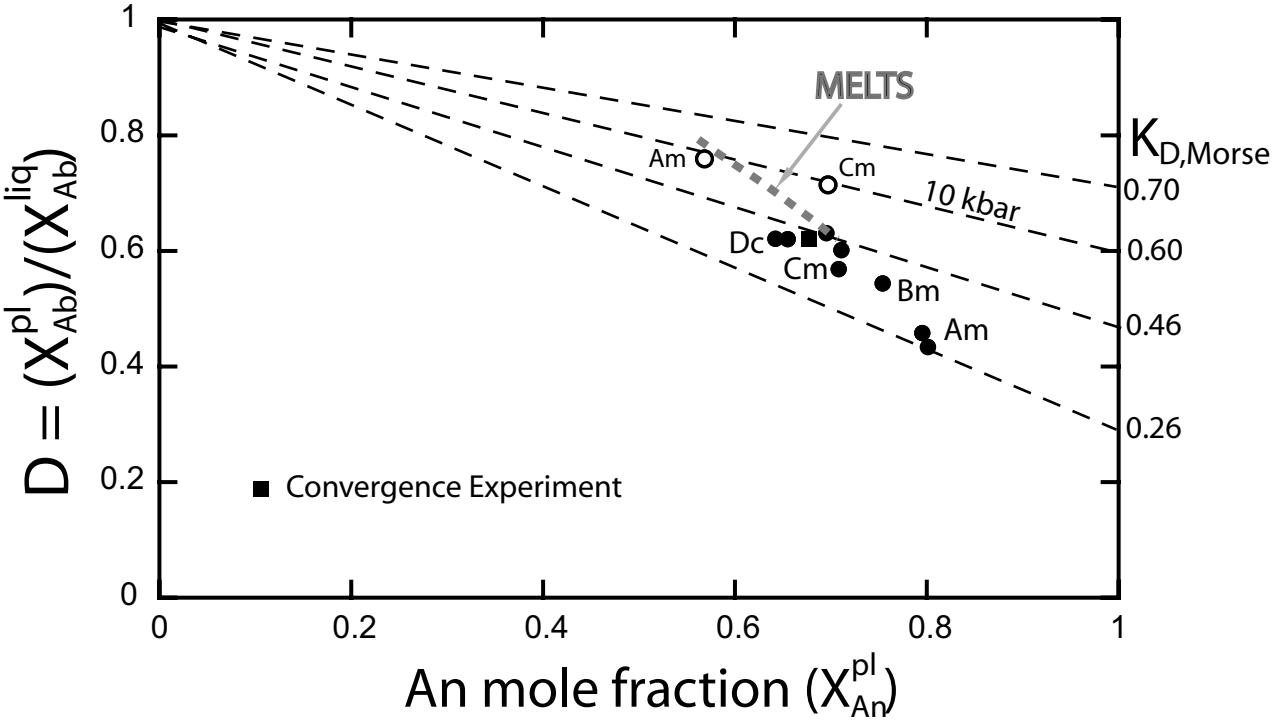
MELTS
Am
Cm
10 kbar
Dc
Cm
Bm
Am
Convergence Experiment
$K_{D,Morse}$
0.70
0.60
0.46
0.26
$D = (X^{pl}_{Ab})/(X^{liq}_{Ab})$
An mole fraction (X^{pl}_{An})
0
0.2
0.4
0.6
0.8
1

Figure 3

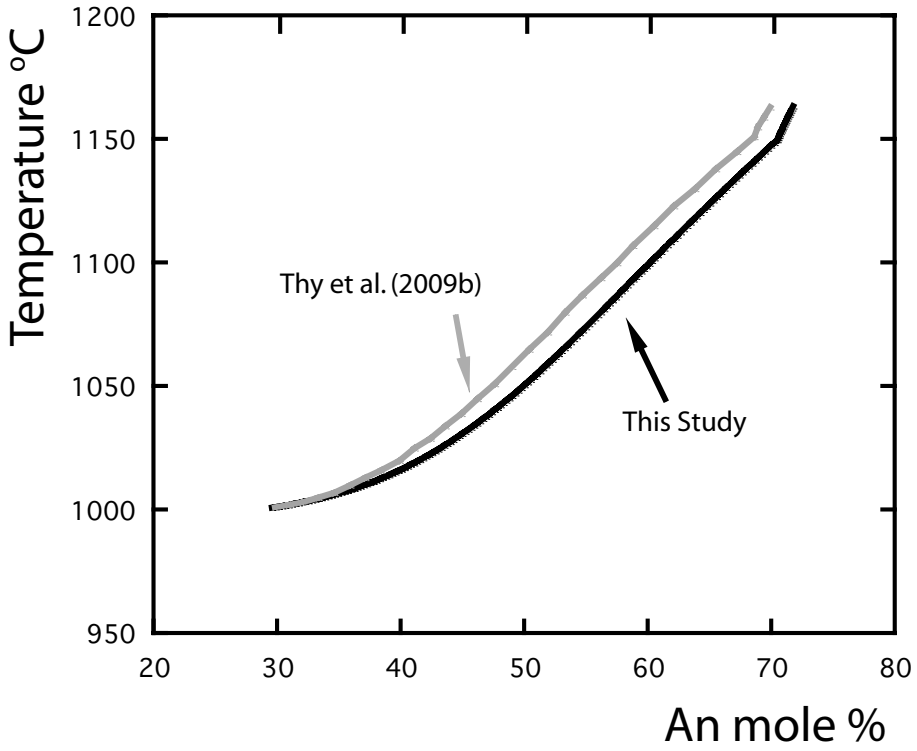
Temperature °C
1200
1150
1100
1050
1000
950
20
30
40
50
60
70
80
An mole %
Thy et al. (2009b)
This Study

Figure 4

This is a preprint, the final version is subject to change, of the American Mineralogist (MSA)
Cite as Authors (Year) Title. American Mineralogist, in press.
(DOI will not work until issue is live.) DOI: http://dx.doi.org/10.2138/am.2013.4044

Table 1. Run conditions for near-liquidus melting experiments on FG1 dikes starting materials (see Thy et al. 2006), and "new" and "old" (Thy et al., 2006) plagioclase analyses for these run products. All experiments are of the "melting" type, where temperature is ramped to T_{dwell} and quenched after t_{dwell}, except FG1Cm-19 that was held at 1177 ºC (~10 º above the liquidus) for 30 minutes and lowered at 500 ºC/hour to a T_{dwell} of 1168 ºC. One gigapascal experiments are new; all 1-atm experiments from Thy et al. (2006).

					This study								‡Thy et al. (2006)							
					*Calculated Modes [New (Old)]				Plag Core		Plag Rim		Plag		Liquid					
Sample	*Run*	*P (GPa)*	*T_{dwell} (ºC)*	*t_{dwell} (Hours)*	*% Melt*	*% Plag*	*% Oliv*	*% Cpx*	†*N*	*An % (1σ)*	†*N*	*An % (1σ)*	†*N*	*An % (1σ)*			*100*Ca/(Ca+Na)*	#*Ca/(Ca+Na) Normative Plag (%)*	§*$K_{D,std}$*	§§*$K_{D,morse}$*
FG1Am	13	0.0001	1173	22	87.2 (86.1)	9.3 (10.2)	3.5 (3.7)	0 (0)	4	70.4 (0.7)	10	80.0 (1.6)	5	70.2 (1.5)	77.2	60.7	0.85	0.40
	9	0.0001	1163	30	81.1 (80.2)	10.6 (11.5)	3.4 (3.6)	4.5 (4.7)	4	68.5 (1.6)	9	80.6 (0.8)	7	69.6 (1.0)	76.8	60.0	0.80	0.38
FG1Bm	13	0.0001	1173	22	87.6 (87.3)	9.5 (9.7)	3.0 (3.0)	0 (0)	5	64.8 (2.6)	11	75.5 (0.9)	6	73.0 (3.6)	74.0	56.2	0.92	0.44
FG1Cm	19	0.0001	1168	29	100	<1	0	0	4	55.6 (6.6)	11	71.4 (0.8)			71.1	53.5	0.99	0.48
	10	0.0001	1163	24	93.9 (93.9)	6.1 (6.1)	0 (0)	0 (0)	6	54.4 (6.4)	11	69.7 (3.3)	5	59.9 (2.4)	70.2	54.3	1.03	0.53
	8	0.0001	1154	42	92.9 (92.7)	6.8 (7.3)	0 (0)	0 (0)	4	57.8 (7.2)	8	71.0 (0.6)	4	57.9 (4.1)	69.6	51.3	0.93	0.44
FG1Dc	4	0.0001	1135	24	92.3 (92.6)	5.4 (5.3)	1.9 (2.1)	0 (0)	7	57.7 (3.7)	11	65.9 (0.8)	6	62.4 (2.4)	66.7	47.6	1.04	0.48
	3	0.0001	1126	67	86.4 (86.6)	9.4 (9.5)	3.7 (3.9)	0 (0)	4	56.6 (5.3)	9	64.6 (0.9)	5	60.0 (5.0)	66.5	40.6	1.09	0.47
FG1Am	1-8	1	1160	23	70.3	5.8	0	24.0	6	62.7 (5.1)	14	70.5 (1.6)	4	68.9 (1.7)	71.5	64.1	1.05	0.78
FG1Cm	1-22	1	1140	94	60.8	10.3	0	28.5	10	50.4 (7.2)	17	57.3 (2.2)	7	56.4 (2.1)	58.0	46.6	1.03	0.67

*Phase proportions (wt. %) estimated by least-squares mixing calculations (see Thy et al., 2006, for details). "New" are modes based on new plagiolcase analyses; "old" in parentheses are those reported by T

†N is the number of analyses comprising averages of cores, rims and possible "mixtures" (from Thy et al., 2006) with one-standard deviation given in parentheses. Anorthite content (An %) given by the Ca/(Ca+Na) ratio on a cation basis x 100.

|| Ca/(Ca+Na) ratio of liquid calculated on a cation basis x 100.

Calculation based on CIPW normative plagioclase components renormalized to 100 % on a cation basis.

‡ Liquid compositions are from Thy et al. (2006), except FG1Cm-19 (Na_2O = 2.43 and CaO = 10.85, wt. %), FG1Am-1-8 (Na_2O = 2.07 and CaO = 9.41, wt. %) and FG1Cm-1-22 (Na_2O = 3.16 and CaO = 7.91, wt. %) from this study.

§ Customary compound Na-Ca distribution coefficient for plagioclase/liquid calculated as the ratio (Na/Ca)pl/(Na/Ca)liq on a cation basis.

§§ Compound partitioning coefficient for Ab and An between plagioclase and liquid calculated from the CIPW normative plagioclase according to Morse (2010) and given on a molecular basis. The liquid compositions are from Thy et al. (2006), except as indicated above.

Table 2. Reversal/convergence experiment for ferrobasaltic magma (East Greenland basalt, GEUS 435068). Melting (JAS-78PT) and dynamic crystallization experiments (JAS-29PTB). All experiments at f_{O2} at $10^{-9.3}$. See text for details.

Run Identification/Sample	Melting ‡ JAS-78PT						Dynamic Crystallization JAS-29PTB				Starting Material 436068
Thermal Regime	|| A						# B				
Final Dwell Temperature (°C	1132						1145				Whole Rock XRF Analysis
Final Dwell Time (hours)	24						76				
	Plag Core	† 1σ N=2	Plag Rim	† 1σ N=7	Glass	† 1σ N=10	Plag Unzoned	† 1σ N=7	Glass	† 1σ N=8	
SiO_2	53.18	1.49	51.41	0.56	47.21	0.32	50.08	0.44	47.23	0.20	47.24
Al_2O_3	29.59	0.78	30.34	0.49	13.28	0.21	30.49	0.30	13.34	0.19	14.24
TiO_2	0.16	0.04	0.18	0.02	4.85	0.07	0.99	0.10	4.52	0.08	4.24
Fe_2O_3	1.00	0.07	1.40	0.27							
FeO					14.51	0.26			13.67	0.30	13.29
MnO					0.21	0.01			0.23	0.10	0.19
MgO	0.13	0.01	0.20	0.03	5.75	0.05	0.10	0.02	6.49	0.09	6.18
CaO	12.06	0.68	13.50	0.28	10.42	0.09	13.64	0.23	10.19	0.24	10.52
Na_2O	4.19	0.49	3.57	0.13	2.61	0.05	3.45	0.14	2.70	0.08	2.76
K_2O	0.26	0.05	0.19	0.02	0.75	0.02	0.09	0.02	0.47	0.12	0.69
P_2O_5					0.53	0.04			0.42	0.06	0.48
Total	100.57		100.79		100.12		98.84		99.26		99.83
* An %	61.4	4.1	67.6	0.6			68.6	0.7			
§ $K_{D,std}$			1.06				0.95				
§§ $K_{D,Morse}$			0.46				0.43				

* Anorthite content (An %) given by the Ca/(Ca+Na) ratio on a cation basis x 100.

‡ JAS-78PT is in addition also saturated in olivine (Fo_{74}).

† 1σ, N is the one-standard deviation and number of analyses comprising averages of cores and rims.

|| A - ramp at >300 ºC/min to (final) dwell temperature and quenching in air after (final) dwell time.

B - ramp at >300 ºC/min to 1190 ºC, dwell for 8h, cool at 5 ºC/min to 1095 ºC, heating at >300 ºC/min to 1175 ºC, cool at 1 ºC/min to 1145 ºC/min, (final) dwell until thermal quenching in water.

Table 3. Summary of plagioclase analyses for near-liquidus melting experiments on FG1 dikes. See Table 1 for experimental conditions and Thy et al. (2006) for details and the compositions of the coexisting phases.

Sample-Run	FG1Am-13				FG1Am-9				FG1Bm-13				FG1Cm-19				FG1Cm-10			
	Core	† 1σ	Rim	† 1σ	Core	† 1σ	Rim	† 1σ	Core	† 1σ	Rim	† 1σ	Core	† 1σ	Rim	† 1σ	Core	† 1σ	Rim	† 1σ
		N=4		N=10		N=4		N=9		N=5		N=11		N=4		N=11		N=6		N=11
SiO_2	51.13	0.15	48.67	0.42	51.94	0.35	48.76	0.42	52.21	0.87	49.26	0.32	55.14	1.96	50.67	0.34	55.51	1.93	51.46	1.02
Al_2O_3	30.61	0.13	32.70	0.33	30.17	0.50	32.03	0.54	29.83	0.34	31.86	0.27	28.26	1.27	31.01	0.51	28.77	1.20	30.30	0.52
TiO_2	0.09	0.01	0.08	0.01	0.10	0.02	0.10	0.04	0.09	0.01	0.08	0.01	0.12	0.02	0.12	0.02	0.11	0.02	0.15	0.02
Fe_2O_3	1.02	0.21	1.07	0.08	1.13	0.09	1.47	0.24	0.94	0.12	1.00	0.09	0.87	0.13	1.30	0.23	0.91	0.14	1.59	0.22
MgO	0.30	0.05	0.26	0.04	0.27	0.03	0.39	0.10	0.20	0.06	0.24	0.02	0.18	0.03	0.30	0.06	0.08	0.02	0.30	0.09
CaO	14.12	0.13	16.05	0.34	13.65	0.33	16.12	0.20	12.87	0.57	15.21	0.18	11.19	1.35	14.42	0.21	10.87	1.35	14.00	0.62
Na_2O	3.28	0.09	2.22	0.17	3.46	0.17	2.14	0.09	3.86	0.28	2.72	0.12	4.94	0.73	3.20	0.09	5.03	0.66	3.36	0.38
K_2O	0.16	0.08	0.15	0.02	0.20	0.06	0.15	0.02	0.17	0.04	0.09	0.01	0.20	0.05	0.10	0.02	0.17	0.04	0.10	0.02
Total	100.71		101.20		100.93		101.15		100.18		100.45		100.91		101.13		101.44		101.25	
An %	70.4	0.7	80.0	1.6	68.5	1.6	80.6	0.8	64.8	2.6	75.5	0.9	55.6	6.6	71.4	0.8	55.6	6.3	71.4	0.8

	FG1Cm-8				FG1Dc-4				FG1Dc-3				FG1Am-1-8				FG1Cm-1-22			
	Core	† 1σ	Rim	† 1σ	Core	† 1σ	Rim	† 1σ	Core	† 1σ	Rim	† 1σ	Core	† 1σ	Rim	† 1σ	Core	† 1o	Rim	† 1σ
		N=4		N=8		N=7		N=11		N=4		N=9		N=6		N=14		N=10		N=17
SiO_2	54.43	2.24	50.64	0.30	54.19	1.05	51.97	0.28	54.45	1.83	52.30	0.23	52.76	1.43	50.65	0.54	55.62	2.04	53.71	0.49
Al_2O_3	28.99	1.41	31.20	0.24	29.36	0.75	30.02	0.91	29.06	1.10	29.90	0.42	29.73	0.98	31.43	0.70	27.82	1.22	29.58	0.45
TiO_2	0.12	0.01	0.11	0.01	0.15	0.03	0.25	0.24	0.11	0.03	0.19	0.11	0.11	0.01	0.08	0.02	0.11	0.02	0.10	0.02
Fe_2O_3	0.86	0.06	1.05	0.06	0.84	0.22	1.37	0.53	0.65	0.06	1.13	0.23	1.00	0.12	0.77	0.19	0.84	0.10	0.58	0.09
MgO	0.15	0.03	0.22	0.02	0.10	0.03	0.29	0.21	0.07	0.01	0.22	0.08	0.24	0.06	0.19	0.09	0.11	0.02	0.08	0.02
CaO	11.52	1.54	14.29	0.19	11.44	0.75	13.17	0.27	11.22	1.18	12.88	0.19	12.57	1.09	14.17	0.30	10.16	1.45	11.53	0.45
Na_2O	4.64	0.74	3.22	0.07	4.63	0.41	3.77	0.07	4.76	0.53	3.90	0.11	4.14	0.55	3.28	0.18	5.53	0.79	4.75	0.25
K_2O	0.18	0.06	0.10	0.01	0.24	0.03	0.15	0.02	0.24	0.03	0.15	0.01	0.26	0.07	0.22	0.06	0.23	0.07	0.21	0.02
Total	100.90		100.82		100.95		100.98		100.56		100.66		100.80		100.79		100.41		100.53	
An %	57.8	7.2	71.0	0.6	57.7	3.7	65.9	0.8	56.6	5.3	64.6	0.1	62.7	5.1	70.5	1.6	50.4	7.2	57.3	2.2

* Anorthite content (An %) given by the Ca/(Ca+Na) ratio on a cation basis x 100.

† 1σ, N is the one-standard deviation and number of analyses comprising averages of cores and rims.